doi:10.1088/2041-8205/739/2/L41

M-BAND IMAGING OF THE HR 8799 PLANETARY SYSTEM USING AN INNOVATIVE LOCI-BASED BACKGROUND SUBTRACTION TECHNIQUE

Raphaël Galicher[1,2], Christian Marois[1], Bruce Macintosh[3], Travis Barman[4], and Quinn Konopacky[3]
[1] National Research Council Canada, Herzberg Institute of Astrophysics, 5071 West Saanich Road, Victoria, BC, V9E 2E7, Canada;
raphael.galicher@nrc-cnrc.gc.ca
[2] Départment de Physique, Université de Montréal, C.P. 6128 Succ. Centre-ville, Montréal, QC, H3C 3J7, Canada
[3] Lawrence Livermore National Laboratory, 7000 East Ave., Livermore, CA 94550, USA
[4] Lowell Observatory, 1400 West Mars Hill Road, Flagstaff, AZ 86001, USA

ABSTRACT

Multi-wavelength observations/spectroscopy of exoplanetary atmospheres are the basis of the emerging exciting field of comparative exoplanetology. The HR 8799 planetary system is an ideal laboratory to study our current knowledge gap between massive field brown dwarfs and the cold 5 Gyr old solar system planets. The HR 8799 planets have so far been imaged at *J*- to *L*-band, with only upper limits available at *M*-band. We present here deep high-contrast Keck II adaptive optics *M*-band observations that show the imaging detection of three of the four currently known HR 8799 planets. Such detections were made possible due to the development of an innovative LOCI-based background subtraction scheme that is three times more efficient than a classical median background subtraction for Keck II AO data, representing a gain in telescope time of up to a factor of nine. These *M*-band detections extend the broadband photometric coverage out to $\sim 5\,\mu$m and provide access to the strong CO fundamental absorption band at $4.5\,\mu$m. The new *M*-band photometry shows that the HR 8799 planets are located near the L/T-type dwarf transition, similar to what was found by other studies. We also confirm that the best atmospheric fits are consistent with low surface gravity, dusty, and non-equilibrium CO/CH_4 chemistry models.

Key words: instrumentation: high angular resolution – methods: data analysis – methods: observational – planetary systems – planets and satellites: atmospheres – techniques: image processing

Online-only material: color figures

1. INTRODUCTION

After more than a decade of searching, the direct exoplanet imaging quest was finally successful in 2008 with the discovery of three planetary systems (Marois et al. 2008b; Kalas et al. 2008; Lagrange et al. 2009). One key advantage of this technique is the detection of the planet's thermal emission. Detailed multi-band photometry and spectrometry can be acquired that can then be compared with atmospheric models to derive the planet's physical characteristics and study the effect of dust and molecular chemistry. With its multiple coeval Jovian planets, the HR 8799 system is an ideal laboratory to study young planets with low temperature/surface gravity atmospheres and bridge the gap between massive field brown dwarfs and the cold solar system planets.

HR 8799 is a 30 Myr old (Marois et al. 2010b; Zuckerman et al. 2011) A5V star located 39.4 pc away (Leeuwen 2007) in the Pegasus constellation. It is classified as a γ Doradus and a λ Bootis star (Gray & Kaye 1999). It also shows an IR excess (Vega-like star) consistent with a debris disk composed of a warm dust disk (6–15 AU), a massive cold dust disk (90–300 AU), and a small dust particle halo extending up to a 1000 AU (Rhee et al. 2007; Su et al. 2009).

Photometry and some spectroscopy of the HR 8799 planets are available in several bands from 1 to 3.8 μm (Marois et al. 2008b, 2010b; Lafrenière et al. 2009; Metchev et al. 2009; Janson et al. 2010; Hinz et al. 2010; Currie et al. 2011; Barman et al. 2011). An initial characterization (Marois et al. 2008b, 2010b; Bowler et al. 2010; Currie et al. 2011; Barman et al. 2011) has been achieved using the available data and state-of-the-art atmospheric models developed for field brown dwarf analysis. It is clear that these planets are quite different than most field brown dwarfs, showing very dusty atmospheres while being cool ($\sim$1000 K) with no sign of methane molecular absorption. *L*- and *M*-band detections/upper limits suggest that this lack of methane is due to a CO/CH_4 non-equilibrium chemistry (Saumon et al. 2003; Cushing et al. 2006; Leggett et al. 2007; Hinz et al. 2010; Bowler et al. 2010; Currie et al. 2011; Barman et al. 2011). Other teams have been able to fit the available photometry with patchy clouds and equilibrium chemistry atmospheres (Marois et al. 2008b; Currie et al. 2011). Accurate *M*-band photometry can help disentangle the various models, but it is hard on a ground-based telescope due to the bright thermal background mainly from the telescope and the adaptive optics system (Lloyd-Hart 2000). This background is particularly hard to remove at Keck, as it varies with time as the instrument image rotator (which is located very near focus) moves and as the AO deformable mirror modulates the rotator-induced background pattern as seen by the detector. As a result, conventional sky/background subtraction routines leave a spatially variable residual that limits final sensitivity.

In this Letter, we present the first *M*-band (4.670 μm) detections of three of the currently four known HR 8799 planets, the longest wavelength at which these planets have been imaged. The observations are discussed in Section 2. The data reduction along with the new very efficient LOCI-based (LOCI: locally optimized combination of images) background subtraction technique are presented in Section 3. Comparisons with field brown dwarfs and new atmospheric fits are shown in Section 5. Conclusions are summarized in Section 6.

2. OBSERVATIONS

The HR 8799 data were obtained on 2009 November 1 and 2 at the Keck II observatory using the adaptive optics system, the NIRC2 near-infrared narrow-field camera (McLean
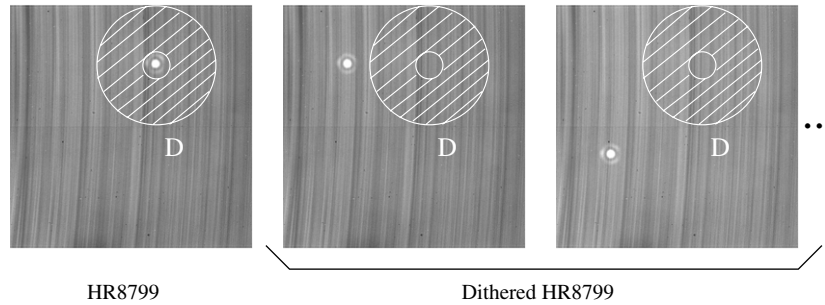
Figure 1. Image I_p where the background has to be subtracted (left) and the D region inside which the LOCI coefficients are optimized using the reference background dither images (right).

& Sprayberry 2003), and the M-band filter ($\lambda_0 = 4.670\,\mu$m and $\Delta\lambda = 0.241\,\mu$m). No coronagraph was used for these observations. For these two nights, 140 unsaturated images (58 for November 1 and 82 for November 2) were acquired, each image consisting of 200 co-adds of 0.3 s, for a total on-source integration time of 140 minutes. The data were taken in angular differential imaging mode (Marois et al. 2006). In that mode, the instrument field rotator is adjusted to track the telescope pupil while leaving the field of view (FOV) to rotate with time. In addition, the telescope was nodded every few minutes between four positions to facilitate the background subtraction. In our data, the total FOV rotation is ∼180 deg for both nights, but both data sets were not acquired through transit (between hour angle [−1.6 hr, −0.4 hr] and [0.6 hr, 1.1 hr] for November 1 and [−1 hr, −0.6 hr] and [0.5 hr, 2.2 hr] for November 2). Although such observing strategy is fine for background limited data, it did limit the amount of speckle subtraction achievable at smaller separations where the data are still speckle noise limited and where planet e is now known to be located (the HR 8799 transit time was actually used during these two nights for L-band imaging to confirm planet e).

3. DATA REDUCTION

The data reduction was performed as follows: we first subtract a dark image, divide by a flat field and mask bad/hot pixels. We then remove known NIRC2 narrow-field camera distortions using the Yelda et al. (2010) solution. The images are rotated by 0.252 deg clockwise to put north up and the plate scale is selected to be 9.952 ± 0002 mas pixel^{-1} to be consistent with the distortion correction of Yelda et al. (2010). After these steps, we subtract the background (Section 3.1) and the speckle noise (Section 3.2) on the two data cubes of 58 (November 1) and 82 (November 2) images separately. We then average the two processed sets to produce a final image.

3.1. LOCI-based Background Subtraction

The telescope was nodded between exposures to record the star at different detector locations. For each image of the sequence, a classical background reduction would consist of subtracting the median of all the images where the star is sufficiently dithered. This standard technique is limited because of the time variations of the thermal background whereas the median uses all the reference background images without distinction. As the background subtraction step is no different than a standard ADI/LOCI speckle subtraction, we have developed a background subtraction routine (Marois et al. 2010a) based on the LOCI algorithm (Lafrenière et al. 2007). This new routine is more efficient than the classical median

subtraction as it puts different weights on the background reference images. Let consider the background subtraction in the pth image I_p of the sequence. An annulus (called D, Figure 1) is defined around the star and all reference background images are selected where the star has been sufficiently dithered compared to I_p. The algorithm searches for the linear combination of these images that minimizes the χ_p^2 (i.e., the residual noise in D excluding bad pixels) which can be expressed as

$$\chi_p^2\big(\alpha_p^{1\leqslant i\leqslant N}\big) = \sum_{i=1}^{N}\sum_{j=1}^{M}\big[\alpha_p^i\, I_i(x_j) - I_p(x_j)\big]^2 D(x_j), \qquad (1)$$

where M is the number of pixels in the image, N is the total number of images in the sequence, x_j is the jth pixel, I_i is the ith image of the sequence, and α_p^i the coefficients to be determined. The inner radius of area D is chosen to avoid the bright star speckle noise that can bias the background minimization algorithm, while its outer radius is chosen to avoid the dithered star images. In our case, the inner and outer radii are 3 and 30 λ/D corresponding to 24 to 240 pixels. We have then imposed $\alpha_p^i = 0$ if the star is at a similar location in I_i as in I_p. The LOCI algorithm then finds the optimal $\alpha_p^{i,\mathrm{best}}$ (Lafrenière et al. 2007; Marois et al. 2010a) that minimizes the χ_p^2. The optimized background image B_p at each pixel for I_p (not only in D) is then

$$B_p = \sum_{i=1}^{N} \alpha_p^{i,\mathrm{best}}\, I_i. \qquad (2)$$

The generated reference background image B_p is finally subtracted from I_p. As $\alpha_p^{i,\mathrm{best}} = 0$ for the images where the star is registered at the same location in I_i as in I_p, B_p does not contain any flux from a possible companion. Moreover, if a companion exists in I_p, its impact on the $\alpha_p^{i,\mathrm{best}}$ LOCI coefficients is negligible since the companion flux is much smaller than the thermal background and D is large compared to the companion point-spread function (PSF).

Once the background is subtracted, we sub-pixel register each image using an iterative cross-correlation Gaussian fit to the PSF core (images are unsaturated).

3.2. Median Speckle Subtraction

The speckle subtraction is performed following a basic ADI data reduction as described in Marois et al. (2006). For each data cube, an initial reference PSF is assembled by taking the median of all images and is then subtracted. We then rotate the images to put north up and median combine them. We apply an unsharp mask to the resulting image (median in a $4 \times 4\lambda/D$
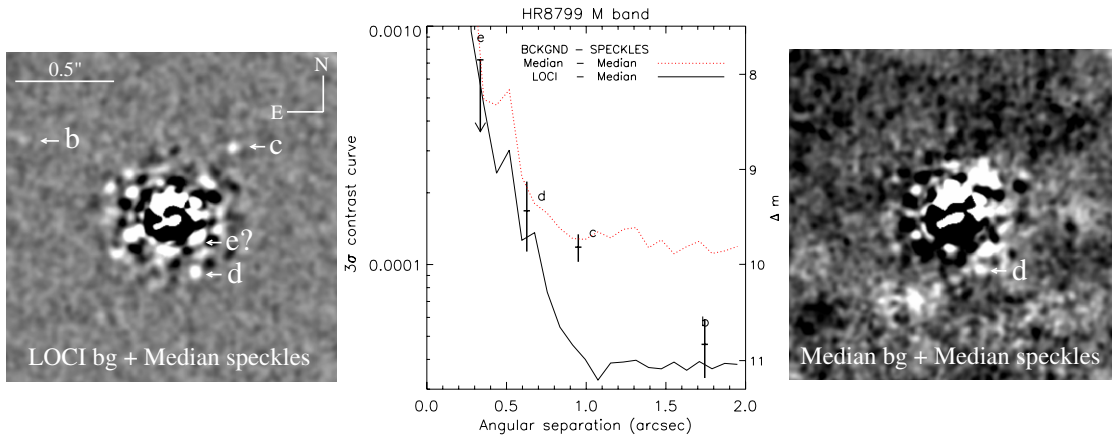
Figure 2. Left panel: final image (average of the November 1 and 2 data) after subtracting the background noise with our new LOCI-based algorithm and the speckle noise with a basic median. Right panel: same reduction, but using a classical median background subtraction. We applied an unsharp mask (median in a $4 \times 4\lambda/D$ box) on the two images and then convolved them by a $0.5\lambda/D$ width Gaussian. The two panels have the same linear intensity scale and FOV. North is up and east is left. Central panel: 3σ radial contrast noise profiles of our resulting median-combined images after subtracting the background with LOCI processing (black full line) or a median (red dashed line). Planets b, c, and d fluxes are also plotted with 1σ error bars along with the planet e flux upper limit.

(A color version of this figure is available in the online journal.)

box) to remove the low spatial frequency noise and convolve it by a $0.5\lambda/D$ width Gaussian to average the high-frequency pixel-to-pixel noise. We finally average the November 1 and 2 images (Figure 2).

Without the LOCI background subtraction, none of the planets would have been detected (right panel, signal-to-noise ratio (S/N) for d is less than 2). With the LOCI background subtraction, HR 8799b, c, and d are detected (left panel, 3–8 S/N). Planet e non-detection is probably due to both sequences not being acquired through transit, thus limiting the amount of speckle noise being removed at small separations from the median subtraction. We tried to apply a more advanced LOCI algorithm (Lafrenière et al. 2007; Marois et al. 2008a, 2010a) to improve the speckle reduction, but as the FOV rotation ranges were small for both nights, no contrast gain was achieved.

4. DATA ANALYSIS

Planet fluxes and positions were obtained by subtracting the planets prior to the speckle reduction using the stellar unsaturated PSF as the template. We also tried subtracting the companions prior to the LOCI-background algorithm and we have confirmed that no bias is introduced by this technique (final flux variations smaller than 0.07%). The subtraction was iterated by moving the planet template and changing its intensity until a minimal noise residual at the planet's location was achieved (inside a $1.5\ \lambda/D$ radius area; Table 1 for the resulting magnitudes). Photometric error bars were calculated in λ/D width annulus. As expected from other wavelengths (Marois et al. 2008b), HR 8799b flux is roughly a third of that of planets c and d. The planet's positions are included in Table 1. The low S/Ns and the large M-band PSF core result in large astrometric errors. A future astrometric HR 8799 paper using shorter wavelength astrometry is in preparation.

Contrast plots (central panel of Figure 2) were obtained by calculating the noise in an annulus having a λ/D width normalized by the stellar PSF flux (after performing the same unsharp mask and convolution of a $0.5\ \lambda/D$ Gaussian). The contrast plots were then normalized at each separation by the estimated point source throughput using simulated ADI median process planets. Figure 2 shows that the LOCI background

Table 1
HR 8799 Planets M-photometry

Planet	b	c	d	e
Separation w.r.t. HR8799a (E,N)″	(1.54, 0.80)	(−0.63, 0.72)	(−0.24, −0.58)	[a]
	±0.019	±0.013	±0.014	
Contrast Δm	10.84 ± 0.30	9.82 ± 0.14	9.44 ± 0.35	>7.85[b]
Absolute M	13.07 ± 0.30	12.05 ± 0.14	11.67 ± 0.35	>10.09[b]
Absolute M (T. Currie et al. 2011, submitted)	>11.37[b]	>11.22[b]	>11.15[b]	
Absolute flux (mJy)	0.91 ± 0.21	2.33 ± 0.25	3.31 ± 0.65	<14.23[b]
Currie's absolute flux (mJy)	<4.36[b]	<5.00[b]	<5.34[b]	

Notes. HR 8799a apparent magnitude is 5.21 and its distance is 39.4 ± 1.0 pc. Magnitude zeropoint is 154 Jy (Cox & Pilachowski 2000).

[a] We use the Marois et al. (2010b) astrometry for planet e.

[b] 3σ upper limits.

subtraction (black full line) is up to ~3 times better than a classical background median subtraction (red dotted line). If a classical background subtraction routine is used, an integration time of up to nine times longer is required to reach the same LOCI background subtraction contrast. This new highly efficient LOCI-based background subtraction routine can be used on any data where the background is non-negligible and evolving with time.

5. DISCUSSIONS

It has been shown that the HR 8799 planets are an L-type extension toward lower effective temperatures and lower surface gravities (Marois et al. 2008b; Bowler et al. 2010; Currie et al. 2011; Barman et al. 2011). The planets have also been found to be dusty with evidence of non-equilibrium CO/CH_4 chemistry. If the HR 8799 planets are plotted in $K' - L'$ versus $L' - M'$ diagram (Figure 3) against field brown dwarfs and lower mass stars (Leggett et al. 2007), it is found that the HR 8799 planets are located near the L/T-type dwarf transition. The M-band photometry is thus consistent with what was found previously by
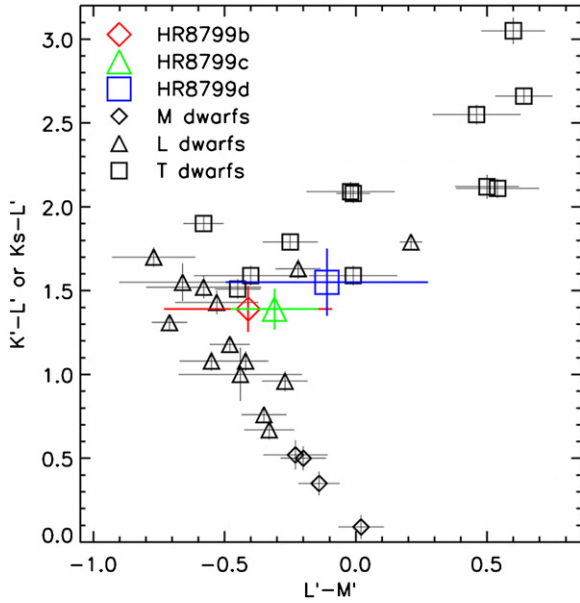
Figure 3. $K-L$ vs. $L-M$ diagram for field brown dwarfs, lower mass stars, and the HR 8799 planets. The planets are located near the end of the L-type sequence, close to the T-type transition.

(A color version of this figure is available in the online journal.)

other studies. From the field brown dwarf best-fit parameters of Figures 4–6 of Leggett et al. (2007), we also find that the planet L- and M-band colors are consistent with dusty atmospheres with vertical mixing. Barman et al. (2011) found a similar result for HR 8799b while considering lower surface gravities.

If we compare our estimated M-band flux to Currie et al. (2011) equilibrium chemistry model predictions, we find that all their best patchy-cloud atmospheric fits are rejected to ∼3σ for HR 8799b. For planets c and d, Currie et al. (2011) use equilibrium chemical models and focus on clouds to interpret the available photometry. The earlier work of Hinz et al. (2010) did compare different chemical models to their M-band upper limits for all three planets, but did not include near-IR photometry. Our new photometry is consistent with some models proposed by the two teams and will help in constraining their fits.

In this Letter, we compare cloudy and non-equilibrium model fits for all of the photometry for the three planets. Such comparison has only been done for planet b so far (Bowler et al. 2010; Barman et al. 2011). Using the same solar-abundance model atmosphere grids and procedures described in Barman et al. (2011), new gravities and effective temperatures are found (Figure 4). For planet b, we find similar model atmosphere parameters as in Barman et al. (2011), but with a slightly higher gravity—$\log(g)$ = 4 rather than 3.5. This solar-abundance model has $T_{\rm eff}$ = 1100 K and, thus, requires a very small
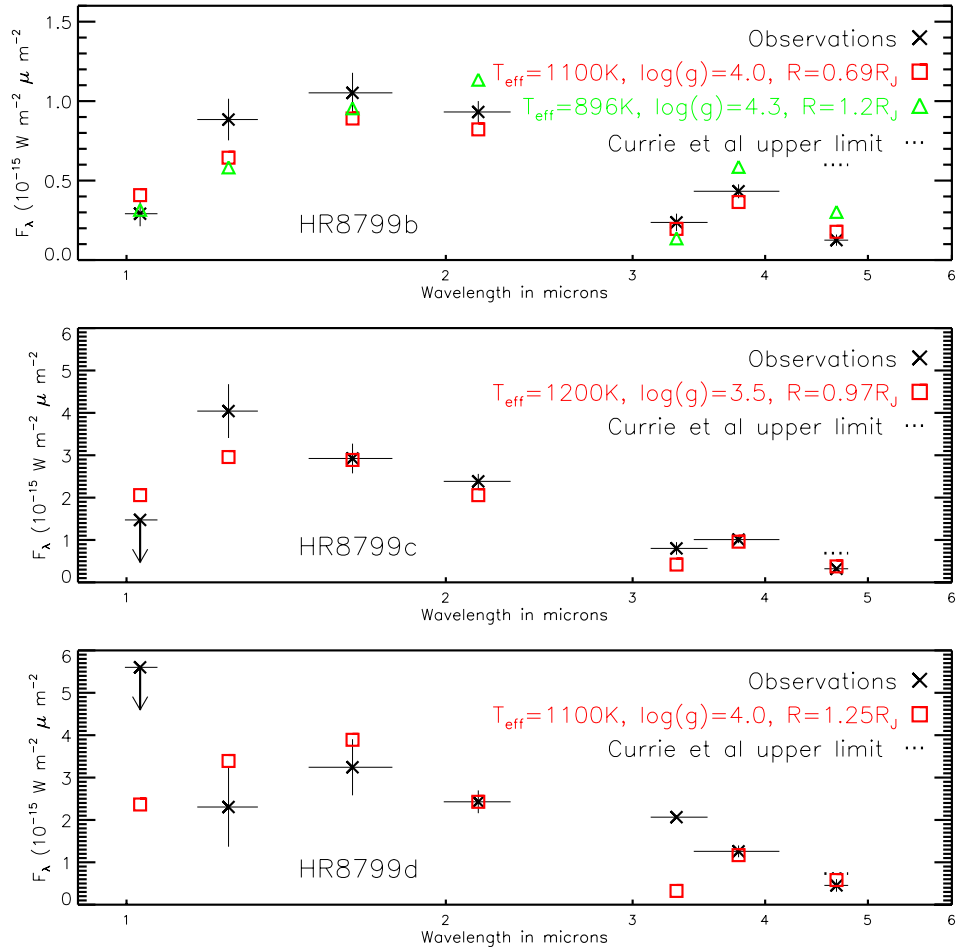
Figure 4. Comparison between the best solar-abundance model (red squares) and the broadband photometry (black cross) for HR 8799b(top), c (middle), and d (bottom). For planet b, the photometry from the 10 times more metal-rich case described in Barman et al. (2011) is plotted in green triangles. The photometric measurements other than for the M-band are from Marois et al. (2008b, 2010b) and Currie et al. (2011). We also show Currie et al. (2011) upper limits for the M-band photometry as a dotted line.

(A color version of this figure is available in the online journal.)

radius ($\sim$0.7 R_j) to match the observed bolometric luminosity; nearly a factor of two smaller than predicted by traditional hot-start models (Baraffe et al. 2003). For planets c and d, we find temperatures and gravities that are fairly close to the expected values from evolution models (Marois et al. 2008b). Barman et al. (2011) argue that increasing the metallicity to 10 times solar could bring the $T_{\rm eff}/\log(g)$ derived from atmosphere and evolution models for planet b into better agreement. The photometry from this metal-rich, evolution-consistent, model is also shown in Figure 4. This model, however, predicts an M-band flux that is 3.5σ brighter than observed (while all other bands agree to 2σ or better). This may indicate an even higher overall metallicity and/or that a non-solar C-to-O ratio is required. A broader exploration of the possible metal abundances for all four planets will be left to a future paper.

6. CONCLUSIONS

In this Letter, we have estimated for the first time the M-band fluxes of three of the currently four known HR 8799 planets. These detections were made possible due to the use of an innovative LOCI-based background subtraction routine that has allowed for a factor of three gain in contrast (factor of nine in integration time) compared to a classical background subtraction using a median. This new background subtraction routine can be used to subtract the background noise in any infrared data.

We have detected HR 8799b, c, and d at M-band from 3 to 8σ. From a $K' - L'$ and $L' - M'$ color diagram, we confirm that the three planets are located near the end of the L-type sequence, close to the L- and T-dwarf transition region. We then derived new atmosphere model fits for the three planets. For planets c and d, temperatures and surface gravities are close to the expected values from evolutionary models. For planet b, the solar-abundance model fits well the broadband photometry from 1 to 5 μm but it requires a very small planetary radius to match the bolometric luminosity and is thus in contradiction with the planet evolution models. The metal-rich evolution-consistent model overpredicts the M-band flux, which may indicate an even higher overall metallicity and/or a non-solar C-to-O ratio. Higher S/N images will help disentangle the different physical and chemical parameters.

REFERENCES

Baraffe, I., Chabrier, G., Barman, T. S., Allard, F., & Hauschildt, P. H. 2003, A&A, 402, 701
Barman, T., Macintosh, B., Konopacky, Q. M., & Marois, C. 2011, ApJ, 733, 65
Bowler, B. P., Liu, M. C., Dupuy, T. J., & Cushing, M. C. 2010, ApJ, 723, 850
Cox, A. N., & Pilachowski, C. A. 2000, Physics Today, 53, 77
Currie, T., Burrows, A., Itoh, Y., et al. 2011, ApJ, 729, 128
Cushing, M. C., Roellig, T. L., Marley, M. S., et al. 2006, ApJ, 648, 614
Gray, R. O., & Kaye, A. B. 1999, AJ, 118, 2993
Hinz, P. M., Rodigas, T. J., Kenworthy, M. A., et al. 2010, ApJ, 716, 417
Janson, M., Bergfors, C., Goto, M., Brandner, W., & Lafrenière, D. 2010, ApJ, 710, L35
Kalas, P., Graham, J. R., Chiang, E., et al. 2008, Science, 322, 1345
Lafrenière, D., Marois, C., Doyon, R., & Barman, T. 2009, ApJ, 694, L148
Lafrenière, D., Marois, C., Doyon, R., Nadeau, D., & Artigau, É. 2007, ApJ, 660, 770
Lagrange, A. M., Gratadour, D., Chauvin, G., et al. 2009, A&A, 493, L21
Leeuwen, E. V. 2007, A&A, 474, 653
Leggett, S., Saumon, D., Marley, M. S., et al. 2007, ApJ, 655, 1079
Lloyd-Hart, M. 2000, PASP, 112, 264
Marois, C., Lafrenière, D., Doyon, R., Macintosh, B., & Nadeau, D. 2006, ApJ, 641, 556
Marois, C., Lafrenière, D., Macintosh, B., & Doyon, R. 2008a, ApJ, 673, 647
Marois, C., Macintosh, B., Barman, T., et al. 2008b, Science, 322, 1348
Marois, C., Macintosh, B., & Véran, J.-P. 2010a, Proc. SPIE, 7736, 77361J
Marois, C., Zuckerman, B., Konopacky, Q. M., Macintosh, B., & Barman, T. 2010b, Nature, 468, 1080
McLean, I. S., & Sprayberry, D. 2003, Proc. SPIE, 4841, 1
Metchev, S., Marois, C., & Zuckerman, B. 2009, ApJ, 705, L204
Rhee, J. H., Song, I., Zuckerman, B., & McElwain, M. 2007, ApJ, 660, 1556
Saumon, D., Marley, M. S., Lodders, K., & Freedman, R. S. 2003, in IAU Symp. 211, Brown Dwarfs, ed. E. Martín (San Francisco, CA: ASP), 345
Su, K. Y. L., Rieke, G. H., Stapelfeldt, K. R., et al. 2009, ApJ, 705, 314
Yelda, S., Lu, J. R., Ghez, A. M., et al. 2010, ApJ, 725, 331
Zuckerman, B., Rhee, J. H., Song, I., & Bessell, M. S. 2011, ApJ, 732, 61